PROCEEDINGS OF SCIENCE

Roy–Steiner equations for pion–nucleon scattering and nucleon resonances[†]

Jacobo Ruiz de Elvira,[a,*] **Martin Hoferichter,**[b] **Bastian Kubis**[c] **and Ulf-G. Meißner**[c,d]

[a] *Universidad Complutense de Madrid, Departamento de Física Teórica and IPARCOS, Facultad de Ciencias Físicas, Plaza de las Ciencias 1, 28040 Madrid, Spain*

[b] *Albert Einstein Center for Fundamental Physics, Institute for Theoretical Physics, University of Bern, Sidlerstrasse 5, 3012 Bern, Switzerland*

[c] *Helmholtz–Institut für Strahlen- und Kernphysik (Theorie) and Bethe Center for Theoretical Physics, Universität Bonn, 53115 Bonn, Germany*

[d] *Institute for Advanced Simulation (IAS-4), Forschungszentrum Jülich, 52425 Jülich, Germany*

In these proceedings, we review the determination of the pion–nucleon scattering amplitude at low energies using Roy–Steiner equations. In particular, we focus on the phenomenological extraction of the pion–nucleon σ-term and address some of the most frequently asked questions regarding our analysis. We also discuss the determination of low-energy constants in chiral perturbation theory, and examine the convergence of the chiral expansion. Finally, we present results for the nucleon resonance pole parameters.

The 11th International Workshop on Chiral Dynamics (CD2024)
26-30 August 2024
Ruhr University Bochum, Germany

[†] These proceedings draw from previous conference contributions [1–6].

[*] Speaker

 ISSN 1824-8039 . Published by SISSA Medialab.

PoS(CD2024)004

Figure 1: (a) LO Feynman diagrams for πN scattering in ChPT. Nucleons are represented by solid lines, and pions by dashed lines. (b) NLO diagrams involving LECs $c_{1\text{–}4}$. These encode the leading effects of $\Delta(1232)$ resonance exchange. Crossed Born terms and explicit Δ exchange diagrams are omitted for brevity.

1. Introduction

Pion–nucleon (πN) scattering is one of the simplest processes to study chiral dynamics involving nucleons. At leading order (LO) in chiral perturbation theory (ChPT)—that is, the expansion in powers of the pion mass (M_π) and momenta—the scattering amplitude is given by the Feynman diagrams shown in Fig. 1. These diagrams lead to the well-known low-energy theorems (LETs) for the S-wave scattering lengths, which are the amplitudes evaluated at threshold [7, 8]:

$$a_{0+}^- = \frac{M_\pi m_N}{8\pi(m_N + M_\pi)F_\pi^2} + O\big(M_\pi^3\big), \qquad a_{0+}^+ = O\big(M_\pi^2\big). \tag{1}$$

The isospin-odd scattering length is predicted solely in terms of M_π, nucleon mass (m_N), and pion decay constant (F_π), while the isospin-even scattering length is suppressed. The strength of the Born term amplitudes—which do not contribute at threshold at LO—is given in terms of the πN coupling constant g, related to the axial coupling g_A via the Goldberger–Treiman relation, $g = g_A m_N / F_\pi$, up to higher orders.

At next-to-leading order (NLO; $O(p^2)$ in the chiral counting), the πN scattering amplitude depends on a set of low-energy constants (LECs), conventionally denoted by $c_{1\text{–}4}$, which are less directly determined from phenomenology. These NLO contributions tend to be large: three of the couplings ($c_{2\text{–}4}$) incorporate the leading low-energy effects of the $\Delta(1232)$ [9], the lowest-lying resonant excitation of the nucleon, see also Fig. 1. As the mass gap is small, $m_\Delta - m_N \simeq 2M_\pi$, and because the Δ couples strongly to the πN system, the numerical values of the NLO LECs are somewhat larger than expected from naive dimensional analysis. Accurately and consistently determining these LECs is crucial, especially given their importance for many nuclear physics applications: as shown in Fig. 2, πN amplitudes provide a significant contribution to the two-pion exchange in nucleon–nucleon (NN) scattering potentials and determine the leading long-range

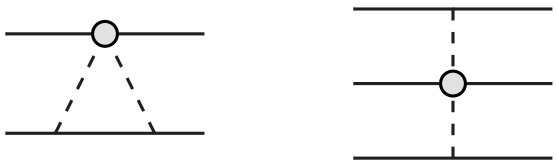

Figure 2: Contributions of πN amplitudes to NN scattering (left) and to the three-nucleon force (right). The gray blob represents subdiagrams of the πN scattering type.

three-nucleon force. Pinning down these amplitudes is therefore one of the main motivations of this project.

Another important motivation is the πN σ-term $\sigma_{\pi N}$, which is defined via the scalar form factor of the nucleon

$$\sigma(t) = \frac{1}{2m_N}\langle N(p')|\hat{m}(\bar{u}u + \bar{d}d)|N(p)\rangle, \qquad \hat{m} = \frac{m_u + m_d}{2}, \qquad \sigma_{\pi N} \equiv \sigma(0), \tag{2}$$

where $t = (p' - p)^2$. The σ-term determines the scalar couplings of the nucleon to u- and d-quarks and thus represents a key matrix element in searches for physics beyond the Standard Model (BSM). This is particularly relevant for interpreting direct-detection dark matter experiments [10–12], as well as for other channels where a scalar current couples to the nucleon [13–15]. While many matrix elements involving currents with no SM probe can only be computed via lattice QCD, the σ-term is an exception. It is linked to πN scattering through the Cheng–Dashen LET [16, 17], which connects the scalar form factor of the nucleon to the Born-term-subtracted isoscalar πN scattering amplitude analytically continued into the unphysical region. Consequently, the phenomenological determination of the σ-term offers a unique opportunity to confront lattice QCD calculations with experimental data. The σ-term also serves as a classic example of chiral dynamics in action. Its smallness results from the cancellation of the LO chiral contribution, while strong $\pi\pi$ rescattering necessitates a resummation within dispersion theory. Accordingly, the scalar channel is of particular interest for BSM applications; see, e.g., Refs. [18–22] for discussions on the implications of chiral symmetry in the context of dark matter searches.

πN scattering is also essential for revealing the spectrum of nucleon resonances, which manifest themselves as distinct peaks in the scattering amplitudes. However, while resonance properties are typically inferred from these peaks [23, 24], a model-independent description of a resonance is uniquely provided by its pole position in the complex energy plane. In practice, this requires performing an analytic continuation from the physical region into the complex plane—a procedure that effectively separates genuine resonance effects from background contributions. A precise dispersive analysis of πN scattering provides rigorous control over the analytic continuation and establishes a systematic framework for connecting experimental data with resonances.

2. Roy–Steiner-equation analysis of pion–nucleon scattering

The Cheng–Dashen LET [16, 17] relates the Born-term-subtracted isoscalar amplitude evaluated at the Cheng–Dashen point ($\nu = 0, t = 2M_\pi^2$) to the scalar form factor of the nucleon, evaluated at momentum transfer $t = 2M_\pi^2$. In practice, this LET is often rewritten as

$$\sigma_{\pi N} = \sigma(0) = \Sigma_d + \Delta_D - \Delta_\sigma - \Delta_R, \tag{3}$$

where Δ_R represents higher-order corrections in the chiral expansion, which are expected to be small given that chiral logarithms cancel at 1-loop order [25]. Δ_σ measures the curvature in the scalar form factor, Δ_D parameterizes contributions to the πN amplitude beyond the first two terms in the subthreshold expansion, and $\Sigma_d = F_\pi^2\left(d_{00}^+ + 2M_\pi^2 d_{01}^+\right)$. As shown in Ref. [26], although these corrections are large individually due to strong rescattering in the isospin-0 $\pi\pi$ S-wave, they cancel to a large extent in the difference. For the numerical analysis we use $\Delta_D - \Delta_\sigma = -1.8(2)$ MeV [27].

In this framework, the remaining information on the πN scattering amplitude is encoded in the subthreshold parameters d_{00}^+ and d_{01}^+, which are determined from the solution of Roy–Steiner (RS) equations [28]. The full system includes both the $\pi N \to \pi N$ (s-channel) and $\pi\pi \to \bar{N}N$ (t-channel) partial waves, with the physical regions of both channels connected through hyperbolic dispersion relations; see Refs. [27, 29] for the derivation and Ref. [30] for the numerical solution. While the underlying principles, analyticity, unitarity, and crossing symmetry in a partial-wave decomposition are identical to those in the Roy equations for $\pi\pi$ scattering [31–34], the presence of the crossed channel in the RS system renders the analysis more akin to that of πK scattering [35] or $\gamma\gamma \to \pi\pi$ [36, 37]. In practice, the solution of the RS equations for πN scattering is significantly stabilized by imposing precise constraints on the S-wave scattering lengths, which are extracted from high-precision measurements of pionic atoms [30, 38, 39]. The final results for the πN partial waves and subthreshold parameters are reported in Ref. [30], while applications to the nucleon form factors are discussed in Refs. [40, 41]. The value of Σ_d, the subthreshold extrapolation of the isoscalar amplitude, can be expressed in a linearized form around the pionic-atom input [42]

$$\Sigma_d = 57.9(9)\,\text{MeV} + \sum_{I_s} c_{I_s} \Delta a_{0+}^{I_s}, \qquad c_{1/2} = 0.242\,\text{MeV}, \qquad c_{3/2} = 0.874\,\text{MeV}, \tag{4}$$

where $\Delta a_{0+}^{I_s}$ gives the deviation from the scattering lengths extracted from pionic atoms in units of $10^{-3} M_\pi^{-1}$. The result for the σ-term itself becomes [42, 43]

$$\sigma_{\pi N} = 59.0(2.0)_{\text{CD}}(2.2)_{\text{IB}}(1.6)_{\text{SL}}(0.9)_{\text{RS}} = 59.0(3.5)\,\text{MeV}, \tag{5}$$

where the various sources of error refer to the Cheng–Dashen remainder, isospin-breaking (IB) corrections in the LET [42], the uncertainty in the scattering lengths, and systematics of the RS solution.

Our central result (5) crucially depends on the πN scattering lengths as extracted from pionic-atom spectroscopy measurements [44–46]. Unfortunately, there is persistent tension with recent results in lattice QCD [47–55], which favor a significantly lower value of $\sigma_{\pi N}$ and can indeed be reinterpreted as another constraint in the scattering-length plane that is inconsistent with the pionic-atom measurements [56]. Given the role of $\sigma_{\pi N}$ as a benchmark for BSM matrix elements, this discrepancy between lattice QCD and phenomenology urgently needs to be resolved.

3. Frequently asked questions

3.1 What if the pionic-atom measurements are wrong?

We believe this is unlikely, given that three independent experimental constraints [44–46] and their theoretical interpretation [38, 39, 57–59] yield an overlapping region for the two scattering lengths. However, further confirmation is highly welcome. An independent constraint can be obtained by fitting a RS representation to low-energy cross-section data [60], which provides an alternative—albeit slightly less precise—determination of the πN scattering lengths. This fit faces several challenges, including substantial normalization uncertainties in the data base. These uncertainties preclude the use of existing compilations, which are biased toward specific fit models, and necessitate careful treatment of IB corrections. In our approach, we analyze each charge

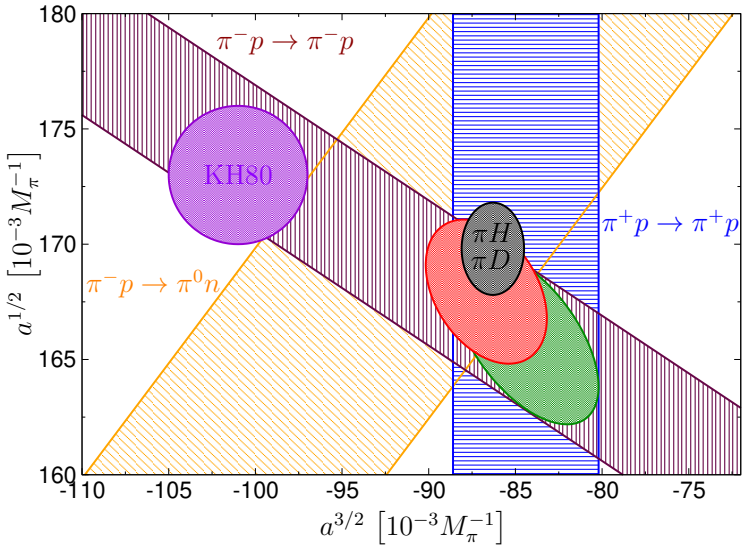

Figure 3: Constraints on the $I_s = 1/2, 3/2$ scattering lengths $a^{1/2}$ and $a^{3/2}$ from $\pi^+ p \to \pi^+ p$ (blue), $\pi^- p \to \pi^- p$ (maroon), and $\pi^- p \to \pi^0 n$ (orange). The combination of the elastic (all) channels leads to the green (red) ellipse. The KH80 and pionic-atom scattering lengths are marked in violet and black, respectively. Figure taken from Ref. [60].

channel separately, treating the corresponding scattering length as a free parameter. We retain the well-established Coulomb correction from Ref. [61] and treat the remaining electromagnetic corrections as an error estimate, while also including all normalization factors as additional free parameters to avoid D'Agostini bias [62] by setting up an iterative fit strategy [63]. The final results for the scattering lengths are shown in Fig. 3. The $\pi^- p \to \pi^- p$ channel is consistent with both the KH80 partial-wave analysis [64] and pionic-atom measurements, and the charge-exchange reaction $\pi^- p \to \pi^0 n$ remains largely inconclusive. In contrast, the $\pi^+ p \to \pi^+ p$ data clearly favor the pionic-atom results. Combining all three channels, we find from the fit to the low-energy cross sections a σ-term of $\sigma_{\pi N} = 58(5)$ MeV, in perfect agreement with Eq. (5).

3.2 Could it be isospin-breaking corrections?

First, since $\sigma_{\pi N}$ is defined as an isosymmetric quantity, one must specify how the isospin limit is taken. For phenomenological applications, this definition conventionally follows the charged-particle masses (see Ref. [65] for $\sigma_{\pi N}$) because most data are available for charged-particle processes, thereby minimizing the need for IB corrections. This choice is particularly relevant for the pion mass; e.g., in the case of the $\pi\pi$ scattering lengths a_0^I, the most precise Roy-equation determination [66] pertains to the charged-pion-mass limit, whereas corrections must be applied when comparing to $K \to 3\pi$ and $K_{\ell 4}$ decays [67, 68]. Enhancements of IB corrections can occur in the presence of neutral-particle thresholds or when the quantity in question vanishes in the chiral limit. This is the case for $\sigma_{\pi N}$, such that IB corrections of size $\Delta_\pi / M_\pi^2 \simeq 6\%$, with $\Delta_\pi = M_\pi^2 - M_{\pi^0}^2$, are expected if the isospin limit is defined instead by the mass of the neutral pion, as preferred in lattice QCD (we denote the corresponding value by $\bar{\sigma}_{\pi N}$). In Ref. [43], we showed that the difference can

be estimated in ChPT as

$$\Delta\sigma_{\pi N} \equiv \sigma_{\pi N} - \bar{\sigma}_{\pi N} = 3.1(5)\,\text{MeV}, \tag{6}$$

which is not negligible when comparing lattice-QCD results with phenomenology [69]. In the updated FLAG review [70], the correction in Eq. (6) is now taken into account, reducing the mismatch between phenomenological and lattice QCD determinations.

Second, enhanced IB corrections can further occur at loop level, which needs to be taken into account for the πN scattering lengths [71–73] entering as input in the solution of the RS equations. Accordingly, IB corrections need to be considered in the analysis of data from pionic atoms to determine these scattering lengths, via level shift [45] and width [46] of pionic hydrogen (πH) as well as the level shift of pionic deuterium (πD) [44], see Fig. 3, together with many-body corrections for πD [57–59, 74–77]. Updating the experimental inputs in Refs. [38, 39], one obtains for the isoscalar and isovector scattering lengths [43]

$$\tilde{a}^+ = 1.7(8)\times 10^{-3} M_\pi^{-1}, \qquad a^- = 86.6(1.0)\times 10^{-3} M_\pi^{-1}, \tag{7}$$

where $\tilde{a}^+$ subsumes a set of universal IB corrections. As input for the master formula for $\sigma_{\pi N}$ derived from the RS analysis [30, 42, 56], in addition, virtual photons need to be subtracted to match the same isospin conventions, leading to isospin-1/2 and -3/2 scattering lengths

$$a^{1/2} = 169.9(2.0)\times 10^{-3} M_\pi^{-1}, \qquad a^{3/2} = -86.5(1.8)\times 10^{-3} M_\pi^{-1}. \tag{8}$$

Finally, to ensure that all corrections are defined with respect to the charged-particle masses, also the Cheng–Dashen theorem requires modifications, reflected by the shifts [42]

$$\begin{aligned}
\Delta_\sigma^p &= \sigma_p\big(2M_\pi^2\big) - \sigma_p = \frac{3g_A^2 M_\pi^3}{64\pi F_\pi^2} + \frac{g_A^2 M_\pi \Delta_\pi}{128\pi F_\pi^2}\Big(-7 + 2\sqrt{2}\log\big(1+\sqrt{2}\big)\Big),\\
\Delta_D^p &= F_\pi^2\Big\{D_p\big(0, 2M_\pi^2\big) - d_{00}^p - 2M_\pi^2 d_{01}^p\Big\} = \frac{23 g_A^2 M_\pi^3}{384\pi F_\pi^2} + \frac{g_A^2 M_\pi \Delta_\pi}{256\pi F_\pi^2}\Big(3 + 4\sqrt{2}\log\big(1+\sqrt{2}\big)\Big),
\end{aligned} \tag{9}$$

in the scalar form factor $\sigma(t)$ and the πN amplitude $D(\nu, t)$, respectively. While all logarithms drop out in the difference, a net effect of $\frac{81 g_A^2 M_\pi \Delta_\pi}{256\pi F_\pi^2} \simeq 3.4$ MeV in $\sigma_{\pi N}$ remains, again a surprisingly large loop correction enhanced by a factor of π that originates from the non-analytic loop functions.

3.3 Excited-state contamination

Despite the small shift in the right direction due to Eq. (6), a significant tension between most lattice-QCD calculations [47–55] (with few exceptions [78]) and phenomenological determinations of $\sigma_{\pi N}$ remains. As shown in Refs. [79–81], excited-state contamination could play an important role in resolving this puzzle, based on the observations that (i) current lattice calculations cannot reliably resolve the spectrum of excited states, especially near the physical point, and (ii) ChPT predicts sizable corrections in the right direction, enhanced by non-analytic loop effects and the $\Delta(1232)$. While it is not yet possible to distinguish between different strategies for excited-state contamination in a statistically significant manner, it is striking that comparing results in Ref. [55] between "window" and "two-state" fit (the latter corresponding better to the ChPT expectation) does entail a systematic increase of (5–10) MeV when restricting results to low pion masses, where no assumptions on SU(3) extrapolations are required and the sensitivity to excited-state effects is indeed expected to be most severe.

a_{0+}^{-} $[10^{-3}M_\pi^{-1}]$	heavy-baryon-NN		heavy-baryon-πN		covariant	
	Δ-less	Δ-ful	Δ-less	Δ-ful	Δ-less	Δ-ful
LO	79.4	79.4	79.4	79.4	79.4	79.4
NLO	79.4	79.4(0)	79.4	79.4(0)	80.1	81.9(1)
N^{2}LO	92.2	92.7(10)	92.9	90.5(9)	89.9	81.7(1.2)
N^{3}LO	68.5	96.3(2.0)	58.6	69.1(1.2)	83.8	83.4(1.0)
Pionic atoms			85.4(9)			

Table 1: Convergence pattern of the isovector scattering length a_{0+}^{-} in two variants of heavy-baryon counting and a covariant formulation, both with and without explicit Δ degrees of freedom. Table taken from Ref. [89].

4. Low-energy constants

The solution of the RS equations naturally proceeds in terms of subthreshold parameters, which offers a unique opportunity for a systematic determination of πN LECs [82]. In fact, since the subthreshold amplitude can be expanded in a polynomial, at a given chiral order there is a one-to-one correspondence between subthreshold parameters and LECs, so that the LECs can be expressed analytically in terms of the subthreshold parameters. Absent any singularities, one would thus expect the chiral expansion to converge best in the subthreshold region. As an added benefit, the subthreshold region is much closer to the kinematics relevant for NN scattering than the physical region for πN. Recent implementations of precision chiral potentials [83, 84] have indeed adopted the accordingly determined LECs.

Surprisingly, though, the chiral convergence of threshold parameters even for the isovector channel is poor for LECs determined at the subthreshold point. The reason for this behavior can be traced back to loop effects enhanced by $g_A^2(c_3 - c_4) \simeq -16\,\text{GeV}^{-1}$ (similar observations pertain to g_A [85] and the axial current [86]), clearly demonstrating that the heavy-baryon amplitude does not converge equally well across the entire low-energy region. The large values of the c_i can be understood from resonance saturation by the $\Delta(1232)$ [9, 87, 88], leading to the expectation that the chiral convergence should improve if the Δ is included as an explicit degree of freedom.

In Ref. [89], we extended the comparison of threshold and subthreshold expansions to the Δ-ful case, both in heavy-baryon and covariant formulations. The results for the isovector scattering length are reproduced in Table 1. The inclusion of the $\Delta(1232)$ indeed improves the convergence, as expected, but in nearly all cases we also observe significant improvements when resumming $1/m_N$ corrections in a covariant set-up. To our knowledge, there is currently no convincing explanation as to why the covariant expansion behaves better. For the application of the LECs to other processes, however, we have now reached the situation where the uncertainties as propagated from the low-energy πN amplitude via the subthreshold parameters are negligible compared to the differences between scheme and chiral order. In Ref. [89], we have made these results available for various schemes up to full one-loop order, with and without explicit Δ degrees of freedom.

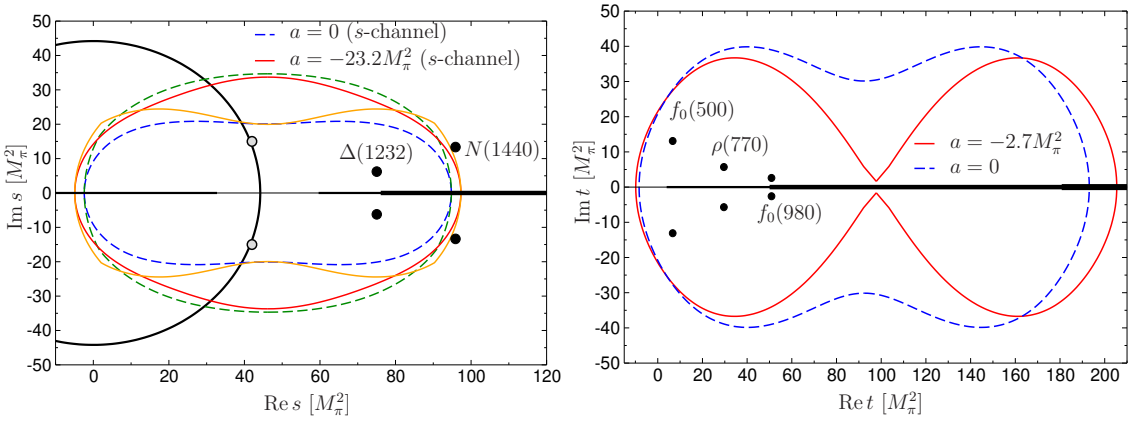

Figure 4: Complex domain of validity for the s-channel (left) and t-channel (right) RS equations. Solid lines show the optimized hyperbola parameters from Ref. [29], while dashed lines correspond to the case $a = 0$. Red and blue lines (for the s-channel) and green and orange lines (for the t-channel) correspond to the constraints imposed by the Lehmann ellipses, and the black lines indicate the various partial-wave cuts. Black dots mark the approximate positions of known resonances, whereas gray circles highlight a subthreshold singularity in the S-wave that lies very close to the circular cut. Figure taken from Ref. [93].

5. Nucleon resonances

The only rigorous, model-independent definition of a resonance is given by its pole position in the complex energy plane on an unphysical Riemann sheet. Unlike Breit–Wigner or K-matrix parameterizations, which rely on specific assumptions, the pole position provides a universal and theoretically well-defined characterization of resonance properties. Accessing unphysical Riemann sheets requires crossing the unitarity cut continuously above a given production threshold, which requires the analytic continuation from the real axis—where experimental data are available—to the complex plane. However, to unambiguously identify a singularity as a physical resonance, it must also have a clear connection to the physical region. The best-known non-trivial example is the $f_0(500)/\sigma$ resonance, a scalar–isoscalar state that appears in $\pi\pi$ scattering with a width comparable to its mass. It is only "visible" as a broad enhancement in the $\pi\pi$ phase shift rather than as a well-defined peak. Its existence and properties were first established by solving $\pi\pi$ scattering at low energies using Roy equations [32, 33] and then performing an analytic continuation based on these solutions [90, 91]. Additionally, its connection to the real axis was confirmed through chiral extrapolation for unphysically heavy pion masses using a unitarized version of ChPT [92].

In the case of nucleon resonances, RS equations provide a powerful framework for performing the analytic continuation based on fundamental principles of analyticity. Moreover, since they are built upon hyperbolic dispersion relations, they naturally couple the s-channel ($\pi N \to \pi N$) and the t-channel ($\pi\pi \to \bar{N}N$) partial waves. This coupling enables a comprehensive study of both s-channel resonances and the residues of resonances contributing to the t-channel processes. The domain of validity of the RS equations in the complex plane [93] is illustrated in Fig. 4. For the optimized hyperbola parameters a, all the key resonances—the $\Delta(1232)$ in the s-channel and the $f_0(500)$, $\rho(770)$, and $f_0(980)$ in the t-channel—are safely contained within this domain. The only notable exception is the Roper $N(1440)$, which lies just beyond the allowed region.

In the case of the $\Delta(1232)$, although it lies near the $\pi\pi N$ threshold, it is, to an excellent approximation, an elastic πN resonance situated on the second Riemann sheet. Consequently, its pole is accessible by continuously crossing the πN unitarity cut, which, together with the Schwarz reflection principle, allows for its study through the corresponding zero in the first Riemann sheet. This property makes the $\Delta(1232)$ ideally suited for a precise determination of its resonance parameters through the analytic continuation of πN RS equations. Defining the resonance mass and width from its pole position as $\sqrt{s}_{\text{pole}} = (M_R - i\frac{\Gamma_R}{2})$, our analysis yields the following values for its mass, width, and residue r [93]:

$$M_R = 1209.5(1.1)\,\text{MeV}, \quad \Gamma_R = 98.5(1.2)\,\text{MeV}, \quad |r| = 51.31(9)\,\text{MeV}, \quad \arg r = -47.4(4)^\circ. \tag{10}$$

While these results agree with previous determinations in the literature [94], the RS approach provides unprecedented control over uncertainties at every stage—both in the low-energy πN amplitudes on the real axis and in their analytic continuation into the complex plane. Nevertheless, at this level of precision, the effects of IB become significant. The pole parameters in Eqs. (10) are given in the isospin limit defined by the elastic reactions $\pi^\pm p \to \pi^\pm p$, as these channels dominate the experimental data. In consequence, the parameters for the $\Delta(1232)$ correspond to a weighted average of the $\Delta^{++} \simeq \pi^+ p$ and the $\Delta^0 \simeq \pi^- p, \pi^0 n$ charge states. The contribution to their mass difference arising from the up-down quark mass difference has been computed in heavy-baryon ChPT at next-to-next-to-leading order [95]. Using the large-N_c constraints on the Δ couplings derived in Ref. [89], this leads to the result:

$$\begin{aligned} m_{\Delta^{++}} - m_{\Delta^0}\Big|_{\text{QCD}} =& \frac{2}{3}(m_p - m_n)\Big|_{\text{QCD}} \times \left\{1 + \frac{2g_A M_\pi^2}{25(4\pi F_\pi)^2}\left[37 + 55\log\left(\frac{M_\pi^2}{\mu^2}\right)\right]\right. \\ &\left. + \frac{4g_A^2\Delta^2}{(4\pi F_\pi)^2}\left[\log\left(\frac{4\Delta^2}{M_\pi^2}\right) - \sigma_\Delta \log\left(\frac{1+\sigma_\Delta}{1-\sigma_\Delta}\right)\right]\right\} \simeq 1.1\,\text{MeV}, \end{aligned} \tag{11}$$

where $\sigma_\Delta = \sqrt{1 - \frac{M_\pi^2}{\Delta^2}}$, Δ is the Δ–N mass splitting in the chiral limit, and $\mu = 770\,\text{MeV}$ is the renormalization scale. The result in Eq. (11) is about half the value quoted in Ref. [94], suggesting that radiative corrections should also play a relevant role in the Δ mass splitting.

Even though the $N(1440)$ lies beyond the domain of validity of the RS equations, applying the same procedure used for the $\Delta(1232)$ results in $M_R = 1473(35)\,\text{MeV}$, $\Gamma_R = 73(14)\,\text{MeV}$, which deviates significantly from the typical Roper parameters [94]. This discrepancy arises because the Roper is an inelastic resonance located on the third Riemann sheet, which is only accessible by continuously crossing the real axis above the $\pi\pi N$ threshold. Thus, the pole in the second Riemann sheet, which lies far from the real axis, is merely a reflection of the true Roper pole.

To properly access the third Riemann sheet, one can perform the analytic continuation using Padé approximants [96–100]. As a cross-check of this method, we apply it to the $\Delta(1232)$, obtaining $M_R = 1209.8(1.5)\,\text{MeV}$, $\Gamma_R = 98.3(1.7)\,\text{MeV}$, $|r| = 51.2(2.2)\,\text{MeV}$, $\delta = -46.8(2.2)^\circ$, which is in excellent agreement with Eq. (10), albeit with slightly larger uncertainties. For the Roper $N(1440)$, our results are [93]:

$$M_R = 1374(3)(4)\,\text{MeV}, \quad \Gamma_R = 215(18)(8)\,\text{MeV}, \quad |r| = 58(15)(17)\,\text{MeV}, \quad \arg r = -65(2)(11)^\circ, \tag{12}$$

where the first uncertainty arises from the RS solution and the second reflects a systematic error associated with the Padé extrapolation. Compared to previous work, our mass parameter lies within the range reported in Ref. [94], though we observe an indication of a slightly larger width.

In addition to the well-known $\Delta(1232)$ and Roper $N(1440)$ resonances, the possible existence of a subthreshold singularity in the $f_{0+}^{1/2}(s)$ partial wave has a long history. It was first noted in meson-exchange models [101] and in unitarized extensions of ChPT [102–104], and more recently in a simplified solution of RS equations [105]. We also confirm a subthreshold pole in the second Riemann sheet of the S_{11} πN wave at $M_R = 913.9(1.6)\,\text{MeV}$, $\Gamma_R = 337.7(6.2)\,\text{MeV}$, which is in good agreement with the results in Ref. [105]. Nevertheless, its interpretation remains unclear: the pole lies deep in the complex plane and nearly touches the circular cut, making it uncertain whether it has any relevance in the physical region. Furthermore, unlike the case of the $f_0(500)$, it seems improbable that chiral extrapolations based on ChPT can bridge this gap, due to the extensive kinematic region involved and the convergence issues of the chiral series in the nucleon sector [30, 89], see Sec. 4.

In contrast to the s-channel resonances, and due to the corresponding unitarity relation, the pole positions of t-channel resonances in the pseudo-physical region are directly used as input in the RS equations, since they are encoded in the corresponding $\pi\pi$ scattering amplitude. Nevertheless, their residues to the $\bar{N}N$ threshold can still be computed, in the scalar channel via [93]

$$\frac{g_{SNN}}{g_{S\pi\pi}} = i\sqrt{6}\frac{\sigma_\pi(t_S)}{4m_N^2 - t_S} f^0_{+,\text{I}}(t_S), \tag{13}$$

where $t_S = \left(M_S - \frac{i\Gamma_S}{2}\right)^2$, and S denotes the scalar resonances $f_0(500)$ and $f_0(980)$. Using Roy-equation dispersive determinations for the corresponding $\pi\pi$ pole parameters, we find

$$g_{f_0(500)NN} = 0.95(19) - 3.48(11)i, \qquad g_{f_0(980)NN} = 0.40(26) - 2.30(15)i. \tag{14}$$

In addition, defining the pion scalar decay constant F_S from the pion scalar form factor, these results allow one to test a generalized Goldberger–Treiman relation in the scalar channel [106, 107], leading to [93]

$$\frac{F_{f_0(500)}\, g_{f_0(500)NN}}{m_N} = 0.90(28) - 2.78(20)i, \qquad \frac{F_{f_0(980)}\, g_{f_0(980)NN}}{m_N} = -1.69(27) - 0.25(15)i, \tag{15}$$

which would be expected to yield unity if the relation were exactly satisfied. Indeed, for the $f_0(500)$, the real part is close to one, but a sizable imaginary part leads to a strong violation of the Goldberger–Treiman relation. Finally, for the vector channel the vector $g^{(1)}_{\rho NN}$ and tensor $\rho(770)$ couplings to the $\bar{N}N$ channel are given by [93]

$$\begin{aligned}
\frac{g^{(1)}_{\rho NN}}{g_{\rho\pi\pi}} &= -2i\sigma_\pi(t_\rho)\frac{m_N q_t^2}{p_t^2}\left[f^1_{+,\text{I}}(t_\rho) - \frac{t_\rho}{4\sqrt{2}\,m_N} f^1_{-,\text{I}}(t_\rho)\right], \\
\frac{g^{(2)}_{\rho NN}}{g_{\rho\pi\pi}} &= 2i\sigma_\pi(t_\rho)\frac{m_N q_t^2}{p_t^2}\left[f^1_{+,\text{I}}(t_\rho) - \frac{m_N}{\sqrt{2}} f^1_{-,\text{I}}(t_\rho)\right].
\end{aligned} \tag{16}$$

Using again the Roy-equation dispersive results for the $\pi\pi$ $\rho(770)$ pole parameters we obtain [93]

$$g^{(1)}_{\rho NN} = 3.31(69) + 2.99(36)i, \quad g^{(2)}_{\rho NN} = 33.4(2.7) + 9.0(1.0)i. \tag{17}$$

These results also allow us to test the universality of the $\rho(770)$ couplings. In particular, one finds

$$\frac{g^{(1)}_{\rho NN}}{g_{\rho\pi\pi}} = 0.50(12) + 0.55(5)i = 0.74(6)e^{0.82(15)i},$$
$$\frac{g^{(2)}_{\rho NN}}{\kappa_v g_{\rho\pi\pi}} = 1.46(12) + 0.54(3)i = 1.55(11)e^{0.35(4)i}, \tag{18}$$

where $\kappa_v = \kappa_p - \kappa_n = 3.706$ is the isovector anomalous magnetic moment of the nucleon. Both expressions are expected to be unity in the narrow-resonance limit, so these deviations highlight a sizable universality violation.

6. Conclusions

In these proceedings, we reviewed RS equations for πN scattering. Regarding phenomenological extractions of the πN σ-term via the Cheng–Dashen LET, there now exist two fully independent determinations—one based on measurements from pionic atoms and the other from low-energy πN cross sections—both of which consistently point to a σ-term value close to 60 MeV. We reported on recent insights regarding IB and excited-state effects, which help in addressing the lingering tension with results from lattice QCD, but the situation remains not fully resolved. We also discussed additional applications of the RS framework. First, we highlighted the determination of LECs by matching the subthreshold amplitude to ChPT. This matching allows for a systematic and model-independent extraction of LECs at various chiral orders, provided together with full covariance matrices in different counting schemes. Second, we examined the role of the RS solution in the extraction of nucleon resonances, yielding precise determinations of the pole parameters of the $\Delta(1232)$ and the Roper resonance, as well as the residues of the t-channel scalar and vector mesons—$f_0(500)$, $f_0(980)$, and $\rho(770)$—in their coupling to $\bar{N}N$.

Acknowledgments

Financial support by the SNSF (Project No. TMCG-2_213690), the Ramon y Cajal program (RYC2019-027605-I) of the Spanish MICIU, and the Spanish Ministerio de Ciencia e Innovacion (Project PID2022-136510NB-C31) is gratefully acknowledged. The work of UGM was supported in part by the CAS President's International Fellowship Initiative (PIFI) (Grant No. 2025PD0022), by the MKW NRW under the funding code No. NW21-024-A, and by ERC AdG EXOTIC (grant No. 101018170).

References

[1] B. Kubis, J. Ruiz de Elvira, M. Hoferichter, and U.-G. Meißner, PoS **CD15**, 021 (2015).

[2] B. Kubis, M. Hoferichter, J. Ruiz de Elvira, and U.-G. Meißner, EPJ Web Conf. **130**, 01006 (2016).

[3] U.-G. Meißner, J. Ruiz de Elvira, M. Hoferichter, and B. Kubis, EPJ Web Conf. **137**, 01014 (2017).

[4] J. Ruiz de Elvira, M. Hoferichter, B. Kubis, and U.-G. Meißner, PoS **Hadron2017**, 141 (2018).

[5] M. Hoferichter, J. Ruiz de Elvira, B. Kubis, and U.-G. Meißner, PoS **CD2018**, 010 (2019).

[6] M. Hoferichter, J. Ruiz de Elvira, B. Kubis, and U.-G. Meißner, PoS **QCHSC24**, 066 (2025).

[7] S. Weinberg, Phys. Rev. Lett. **17**, 616 (1966).

[8] Y. Tomozawa, Nuovo Cim. A **46**, 707 (1966).

[9] V. Bernard, N. Kaiser, and U.-G. Meißner, Nucl. Phys. A **615**, 483 (1997).

[10] A. Bottino, F. Donato, N. Fornengo, and S. Scopel, Astropart. Phys. **13**, 215 (2000).

[11] J. R. Ellis, K. A. Olive, and C. Savage, Phys. Rev. D **77**, 065026 (2008).

[12] A. Crivellin, M. Hoferichter, and M. Procura, Phys. Rev. D **89**, 054021 (2014).

[13] V. Cirigliano, R. Kitano, Y. Okada, and P. Tuzon, Phys. Rev. D **80**, 013002 (2009).

[14] A. Crivellin, M. Hoferichter, and M. Procura, Phys. Rev. D **89**, 093024 (2014).

[15] J. de Vries, E. Mereghetti, C.-Y. Seng, and A. Walker-Loud, Phys. Lett. B **766**, 254 (2017).

[16] T. P. Cheng and R. F. Dashen, Phys. Rev. Lett. **26**, 594 (1971).

[17] L. S. Brown, W. J. Pardee, and R. D. Peccei, Phys. Rev. D **4**, 2801 (1971).

[18] V. Cirigliano, M. L. Graesser, and G. Ovanesyan, JHEP **10**, 025 (2012).

[19] M. Hoferichter, P. Klos, and A. Schwenk, Phys. Lett. B **746**, 410 (2015).

[20] M. Hoferichter, P. Klos, J. Menéndez, and A. Schwenk, Phys. Rev. D **94**, 063505 (2016).

[21] M. Hoferichter, P. Klos, J. Menéndez, and A. Schwenk, Phys. Rev. Lett. **119**, 181803 (2017).

[22] M. Hoferichter, P. Klos, J. Menéndez, and A. Schwenk, Phys. Rev. D **99**, 055031 (2019).

[23] F. Gross *et al.*, Eur. Phys. J. C **83**, 1125 (2023).

[24] M. Battaglieri *et al.*, Acta Phys. Polon. B **46**, 257 (2015).

[25] V. Bernard, N. Kaiser, and U.-G. Meißner, Phys. Lett. B **389**, 144 (1996).

[26] J. Gasser, H. Leutwyler, and M. E. Sainio, Phys. Lett. B **253**, 260 (1991).

[27] M. Hoferichter, C. Ditsche, B. Kubis, and U.-G. Meißner, JHEP **06**, 063 (2012).

[28] G. E. Hite and F. Steiner, Nuovo Cim. A **18**, 237 (1973).

[29] C. Ditsche, M. Hoferichter, B. Kubis, and U.-G. Meißner, JHEP **06**, 043 (2012).

[30] M. Hoferichter, J. Ruiz de Elvira, B. Kubis, and U.-G. Meißner, Phys. Rept. **625**, 1 (2016).

[31] S. M. Roy, Phys. Lett. B **36**, 353 (1971).

[32] B. Ananthanarayan, G. Colangelo, J. Gasser, and H. Leutwyler, Phys. Rept. **353**, 207 (2001).

[33] R. García-Martín *et al.*, Phys. Rev. D **83**, 074004 (2011).

[34] I. Caprini, G. Colangelo, and H. Leutwyler, Eur. Phys. J. C **72**, 1860 (2012).

[35] P. Büttiker, S. Descotes-Genon, and B. Moussallam, Eur. Phys. J. C **33**, 409 (2004).

[36] M. Hoferichter, D. R. Phillips, and C. Schat, Eur. Phys. J. C **71**, 1743 (2011).

[37] M. Hoferichter and P. Stoffer, JHEP **07**, 073 (2019).

[38] V. Baru *et al.*, Phys. Lett. B **694**, 473 (2011).

[39] V. Baru *et al.*, Nucl. Phys. A **872**, 69 (2011).

[40] M. Hoferichter *et al.*, Eur. Phys. J. A **52**, 331 (2016).

[41] M. Hoferichter, B. Kubis, J. Ruiz de Elvira, and P. Stoffer, Phys. Rev. Lett. **122**, 122001 (2019), [Erratum: Phys. Rev. Lett. **124**, 199901 (2020)].

[42] M. Hoferichter *et al.*, Phys. Rev. Lett. **115**, 092301 (2015).

[43] M. Hoferichter *et al.*, Phys. Lett. B **843**, 138001 (2023).

[44] Th. Strauch *et al.*, Eur. Phys. J. A **47**, 88 (2011).

[45] M. Hennebach *et al.*, Eur. Phys. J. A **50**, 190 (2014), [Erratum: Eur. Phys. J. A **55**, 24 (2019)].

[46] A. Hirtl *et al.*, Eur. Phys. J. A **57**, 70 (2021).

[47] S. Dürr *et al.* (BMWc), Phys. Rev. Lett. **116**, 172001 (2016).

[48] Y.-B. Yang *et al.* (χQCD), Phys. Rev. D **94**, 054503 (2016).

[49] A. Abdel-Rehim *et al.* (ETM), Phys. Rev. Lett. **116**, 252001 (2016).

[50] G. S. Bali *et al.* (RQCD), Phys. Rev. D **93**, 094504 (2016).

[51] N. Yamanaka *et al.* (JLQCD), Phys. Rev. D **98**, 054516 (2018).

[52] C. Alexandrou *et al.* (ETM), Phys. Rev. D **102**, 054517 (2020).

[53] Sz. Borsanyi *et al.* (BMWc), (2020), arXiv:2007.03319 [hep-lat].

[54] G. S. Bali *et al.* (RQCD), JHEP **05**, 035 (2023).

[55] A. Agadjanov *et al.*, Phys. Rev. Lett. **131**, 261902 (2023).

[56] M. Hoferichter, J. Ruiz de Elvira, B. Kubis, and U.-G. Meißner, Phys. Lett. B **760**, 74 (2016).

[57] V. Lensky *et al.*, Phys. Lett. B **648**, 46 (2007).

[58] V. Baru *et al.*, Phys. Lett. B **659**, 184 (2008).

[59] V. Baru *et al.*, Eur. Phys. J. A **48**, 69 (2012).

[60] J. Ruiz de Elvira, M. Hoferichter, B. Kubis, and U.-G. Meißner, J. Phys. G **45**, 024001 (2018).

[61] B. Tromborg, S. Waldenstrøm, and I. Øverbø, Phys. Rev. D **15**, 725 (1977).

[62] G. D'Agostini, Nucl. Instrum. Meth. A **346**, 306 (1994).

[63] R. D. Ball *et al.* (NNPDF), JHEP **05**, 075 (2010).

[64] R. Koch and E. Pietarinen, Nucl. Phys. A **336**, 331 (1980).

[65] U.-G. Meißner and S. Steininger, Phys. Lett. B **419**, 403 (1998).

[66] G. Colangelo, J. Gasser, and H. Leutwyler, Nucl. Phys. B **603**, 125 (2001).

[67] G. Colangelo, J. Gasser, and A. Rusetsky, Eur. Phys. J. C **59**, 777 (2009).

[68] M. Bissegger, A. Fuhrer, J. Gasser, B. Kubis, and A. Rusetsky, Nucl. Phys. B **806**, 178 (2009).

[69] Y. Aoki *et al.* (FLAG), Eur. Phys. J. C **82**, 869 (2022).

[70] Y. Aoki *et al.* (FLAG), (2024), arXiv:2411.04268 [hep-lat].

[71] J. Gasser *et al.*, Eur. Phys. J. C **26**, 13 (2002).

[72] M. Hoferichter, B. Kubis, and U.-G. Meißner, Phys. Lett. **B678**, 65 (2009).

[73] M. Hoferichter, B. Kubis, and U.-G. Meißner, Nucl. Phys. A **833**, 18 (2010).

[74] S. Weinberg, Phys. Lett. B **295**, 114 (1992).

[75] S. R. Beane *et al.*, Nucl. Phys. A **720**, 399 (2003).

[76] V. Baru *et al.*, Phys. Lett. B **589**, 118 (2004).

[77] S. Liebig, V. Baru, F. Ballout, C. Hanhart, and A. Nogga, Eur. Phys. J. A **47**, 69 (2011).

[78] C. Alexandrou *et al.*, Phys. Rev. D **90**, 074501 (2014).

[79] R. Gupta, S. Park, M. Hoferichter, E. Mereghetti, B. Yoon, and T. Bhattacharya, Phys. Rev. Lett. **127**, 242002 (2021).

[80] R. Gupta, T. Bhattacharya, M. Hoferichter, E. Mereghetti, S. Park, and B. Yoon, PoS **CD2021**, 060 (2024).

[81] S. Park *et al.*, (2025), arXiv:2503.07100 [hep-lat].

[82] M. Hoferichter, J. Ruiz de Elvira, B. Kubis, and U.-G. Meißner, Phys. Rev. Lett. **115**, 192301 (2015).

[83] D. R. Entem, R. Machleidt, and Y. Nosyk, Phys. Rev. C **96**, 024004 (2017).

[84] P. Reinert, H. Krebs, and E. Epelbaum, Eur. Phys. J. A **54**, 86 (2018).

[85] Z. B. Hall *et al.*, (2025), arXiv:2503.09891 [hep-lat].

[86] M. Hoferichter, J. Menéndez, and A. Schwenk, Phys. Rev. D **102**, 074018 (2020).

[87] V. Bernard, N. Kaiser, and U.-G. Meißner, Int. J. Mod. Phys. **E04**, 193 (1995).

[88] T. Becher and H. Leutwyler, Eur. Phys. J. C **9**, 643 (1999).

[89] D. Siemens *et al.*, Phys. Lett. B **770**, 27 (2017).

[90] I. Caprini, G. Colangelo, and H. Leutwyler, Phys. Rev. Lett. **96**, 132001 (2006).

[91] R. García-Martin *et al.*, Phys. Rev. Lett. **107**, 072001 (2011).

[92] C. Hanhart, J. R. Peláez, and G. Ríos, Phys. Rev. Lett. **100**, 152001 (2008).

[93] M. Hoferichter, J. Ruiz de Elvira, B. Kubis, and U.-G. Meißner, Phys. Lett. B **853**, 138698 (2024).

[94] S. Navas *et al.* (Particle Data Group), Phys. Rev. D **110**, 030001 (2024).

[95] B. C. Tiburzi and A. Walker-Loud, Nucl. Phys. A **764**, 274 (2006).

[96] P. Masjuan and J. J. Sanz-Cillero, Eur. Phys. J. C **73**, 2594 (2013).

[97] P. Masjuan, J. Ruiz de Elvira, and J. J. Sanz-Cillero, Phys. Rev. D **90**, 097901 (2014).

[98] I. Caprini *et al.*, Phys. Rev. D **93**, 076004 (2016).

[99] J. R. Peláez, A. Rodas, and J. Ruiz de Elvira, Eur. Phys. J. C **77**, 91 (2017).

[100] L. von Detten, F. Noël, C. Hanhart, M. Hoferichter, and B. Kubis, Eur. Phys. J. C **81**, 420 (2021).

[101] M. Döring *et al.*, Nucl. Phys. A **829**, 170 (2009).

[102] M. Döring and K. Nakayama, Eur. Phys. J. A **43**, 83 (2010).

[103] Y.-F. Wang, D.-L. Yao, and H.-Q. Zheng, Eur. Phys. J. C **78**, 543 (2018).

[104] Q.-Z. Li and H.-Q. Zheng, Commun. Theor. Phys. **74**, 115203 (2022).

[105] X.-H. Cao, Q.-Z. Li, and H.-Q. Zheng, JHEP **12**, 073 (2022).

[106] R. J. Crewther and L. C. Tunstall, Phys. Rev. D **91**, 034016 (2015).

[107] R. Zwicky, Phys. Rev. D **110**, 014048 (2024).